Geophysical Research Letters

RESEARCH LETTER
10.1029/2018GL078130

Special Section:
Cassini's Final Year: Science Highlights and Discoveries

Enceladus Auroral Hiss Emissions During Cassini's Grand Finale

A. H. Sulaiman[1], W. S. Kurth[1], G. B. Hospodarsky[1], T. F. Averkamp[1], S.-Y. Ye[1], J. D. Menietti[1], W. M. Farrell[2], D. A. Gurnett[1], A. M. Persoon[1], M. K. Dougherty[3], and G. J. Hunt[3]

[1]Department of Physics and Astronomy, University of Iowa, Iowa City, IA, USA, [2]NASA Goddard Space Flight Center, Greenbelt, MD, USA, [3]Blackett Laboratory, Imperial College London, London, UK

Abstract Cassini's Radio and Plasma Wave Science (RPWS) instrument detected intense auroral hiss emissions during one of its perikrone passes of the Grand Finale orbits. The emissions were detected when Cassini traversed a flux tube connected to Enceladus' orbit (L-shell = 4) and at a time when both the spacecraft and the icy moon were in similar longitudes. Previous observations of auroral hiss related to Enceladus were made only during close flybys and here we present the first observation of such emissions close to Saturn. Further, ray-tracing analysis shows the source location at a latitude of 63°, in excellent agreement with earlier UVIS observations of Enceladus' auroral footprint by Pryor et al. (2011, https://doi.org/10.1038/nature09928). The detection has been afforded exclusively by the Grand Finale phase, which enabled sampling of Enceladus' high-latitude flux tube near Saturn. This result provides new insight into the spatial extent of the electrodynamic interaction between Saturn and Enceladus.

Plain Language Summary Cassini's high-inclination Grand Finale orbits brought the spacecraft closer to Saturn than ever before, with the closest approach between the cloud tops and the inner edge of the D ring. This unprecedented set of orbits introduced a new view of Saturn's system by enabling direct measurements of high-latitude Enceladus flux tubes close to Saturn. Here we present evidence of communication between Saturn's ionosphere and Enceladus during the Grand Finale orbits, revealing the vast spatial extent of their coupling via plasma waves.

Key Points:
- Complex whistler mode auroral hiss emissions were detected during the Grand Finale
- Emissions were detected on the Enceladus flux tube, and for the first time, not local to Enceladus but very close to Saturn
- Source region is co-located with previous observations of Enceladus' auroral hot spot

Supporting Information:
- Supporting Information S1
- Figure S1

Correspondence to:
A. H. Sulaiman,
ali-sulaiman@uiowa.edu

Citation:
Sulaiman, A. H., Kurth, W. S., Hospodarsky, G. B., Averkamp, T. F., Ye, S.-Y., Menietti, J. D., et al. (2018). Enceladus auroral hiss emissions during Cassini's Grand Finale. *Geophysical Research Letters*, *45*, 7347–7353. https://doi.org/10.1029/2018GL078130

Received 28 MAR 2018
Accepted 1 JUN 2018
Accepted article online 7 JUN 2018
Published online 14 AUG 2018

©2018. American Geophysical Union. All Rights Reserved.

1. Introduction

In September 2017, the Cassini spacecraft concluded its 13-year mission at Saturn in a controlled deorbit by atmospheric entry. This was preceded by 22 highly inclined "Grand Finale" orbits with periapsides between the cloud tops and inner edge of the D ring. This trajectory granted large latitudinal coverage as well as unrivaled proximity to the giant planet over an orbital period of ~6.5 days. First in situ measurements of the ionosphere have revealed intense plasma waves and large variability in electron density of up to 2 orders of magnitude as well as a north-south asymmetry attributed to the shadow cast by Saturn's A and B rings (Menietti et al., 2018; Persoon et al., 2018; Sulaiman et al., 2017, this issue; Wahlund et al., 2018).

In this letter, we report observations of strong whistler mode emissions that are directly associated with Saturn's dynamic icy moon, Enceladus, as detected by the Radio and Plasma Wave Science (RPWS) instrument during the Grand Finale. Enceladus is a dominant player in the dynamics of Saturn's magnetosphere as a continuous source of neutrals and dust (Dougherty et al., 2006; Spahn et al., 2006). During flybys of the icy moon, the RPWS instrument detected whistler mode waves in the electric field frequency-time spectrogram (Gurnett et al., 2011). This class of emissions is often called auroral hiss, although the emissions are not always linked to the auroral regions. They are characterized by their funnel or V-shaped features in the electric field frequency-time spectrogram (hence sometimes called "saucers"), and irrespective of their source, they are all believed to be propagating in the whistler mode and are understood to be generated via Landau resonance in the presence of electron beams (Gurnett et al., 1983; James, 1976). Saturn's environment is known for the ubiquity of auroral hiss emissions associated with diverse sources, namely, the planet (Kopf et al., 2010), the rings (Xin, Gurnett, Santolík, et al., 2006; Sulaiman et al., 2018, this issue), and most notably Enceladus (Gurnett et al., 2011; Leisner et al., 2013). Using ray-tracing analyses, the latter authors concluded that the emissions are generated by electron beams accelerated close to Enceladus. Here, however, we report an intense auroral hiss emission during the Grand Finale phase when Cassini entered previously unvisited regions, farther from Enceladus and much closer to Saturn than previous detections. Repeated

detection of auroral hiss associated with Enceladus underlines pronounced electrodynamic coupling between Saturn and its icy satellite. Moreover, the observation reported here particularly reveals the vast spatial extent of Enceladus' influence in the context of wave-particle processes operating in Saturn's magnetosphere.

2. Observations

Auroral hiss is one of the most commonly observed plasma waves in planetary magnetospheres. It propagates in the whistler mode, which has an upper frequency cutoff at the lower of the electron plasma frequency, f_{pe}, and the electron cyclotron frequency, f_{ce}. Their characteristic funnel or V-shaped spectral feature is attributed to a propagation effect of whistler mode waves, whereby the wave normal vector makes an angle to the background magnetic field that is dependent on frequency, as governed by the dispersion relation (Gurnett, 1966; Stix, 1992). Auroral hiss emissions are typically produced by quasi-electrostatic whistler mode waves, which are limited to propagating along the resonance cone. The resulting raypath (i.e., group velocity) angle with respect to the magnetic field, ψ_{res}, is simplified to

$$\cos^2\psi_{res} \simeq \frac{\left(f_{pe}^2 - f^2\right)\left(f_{ce}^2 - f^2\right)}{f_{pe}^2 f_{ce}^2} \quad (1)$$

as derived by Stix (1992) from the appropriate elements of the dielectric tensor in the cold plasma approximation. This neglects ion effects because the frequencies are generally sufficiently high that the ions play no role in this wave's propagation. It can be seen that at lower frequencies, the raypath angle becomes more parallel to the magnetic field line and, conversely, becomes monotonically more perpendicular with higher frequencies until f approaches min $\{f_{pe}, f_{ce}\}$. The consequence is higher frequencies being detected farther away from the source magnetic field line and progressively lower frequencies being detected as the spacecraft approaches the source magnetic field line. This explains the V-shaped feature on a frequency-time spectrogram. However, this can be more ambiguous if the spacecraft trajectory is nearly parallel to the source magnetic field line.

The electric field-measuring component of the RPWS instrument comprises a set of three 10 m antennas in a triaxial arrangement. For the purpose of this study, we use high-resolution data provided by the wideband receiver, which has a frequency upper limit of 10.5 kHz. The spectral resolution was 13.6 Hz, and the temporal resolution was 125 ms/spectrum. A five-channel Waveform Receiver (WFR) provided coarse electric and magnetic field power spectra up to a frequency of 2.5 kHz. This ensemble allowed for distinguishing between electrostatic and electromagnetic emissions. More details on the RPWS instrument, particularly a schematic of the triaxial electric antennae arrangement, can be found in Gurnett et al. (2004).

The spacecraft's positions during the observations of the apices (or centers) of the two auroral hiss events presented here are illustrated in Figure 1a with the L-shell concerning Enceladus' orbit overlaid, and an equatorial projection in Figure 1b as well as the respective locations of Enceladus at the times the events were recorded. The L-shell is that of a simple dipole with a displacement of 0.037 Rs north of the equatorial plane (1 R_S = 60,268 km; Saturn radius; Dougherty et al., 2004). For both events, it is clear that the auroral hiss emissions were detected when Cassini traversed flux tubes connected to Enceladus. The first observation ("Event 1") was recorded on 27 November 2016—a few months before the commencement of the Grand Finale orbits—and its spectrogram is shown in Figure 2. The apex of the emission was at 191 R_E from Enceladus (1 R_E = 252 km; Enceladus radius), at a kronographic latitude of 11.9°, and longitude of 4.7°. At the same time, Enceladus was at a longitude of 4.5°. This emission is a classic example of an auroral hiss saucer observed in the vicinity of Enceladus (e.g., Gurnett et al., 2011). The second observation ("Event 2") was recorded on 2 September 2017 during the Grand Finale phase—two weeks before the end of the mission—and its spectrogram is shown in Figure 4. The spectral feature of Event 2 is much more detailed in structure, and its apex was much farther from Enceladus at 776 R_E and very close to Saturn at 0.55 R_S from its surface with a kronographic latitude of 53.2°and longitude of 54.0°. At the same time, Enceladus was at a longitude of 56.9°. Here the emission at the time of detection was therefore leading Enceladus by 2.9° in longitude. This is because the footpoint of the Enceladus flux tube anchored at Saturn's ionosphere undergoes a

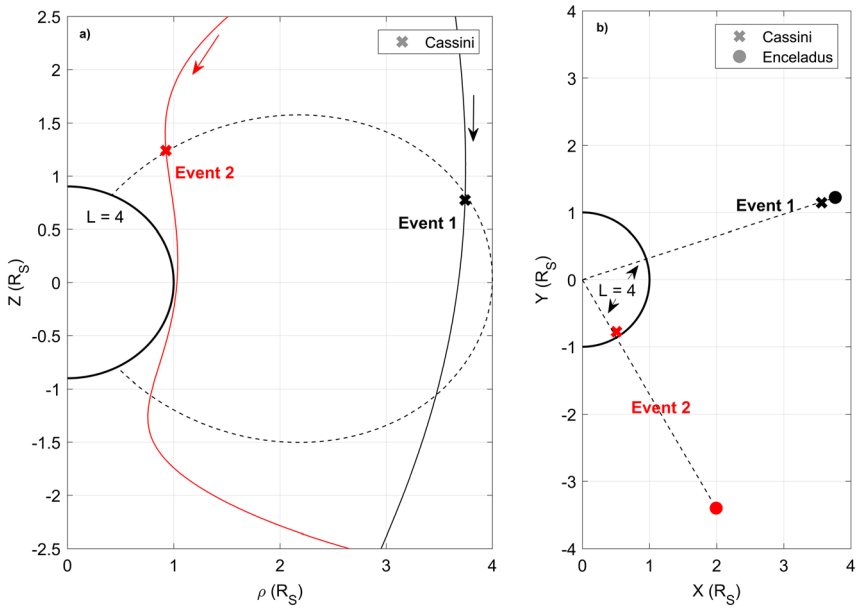

Figure 1. (a) Positions of Cassini (crosses) during Event 1 (black) and Event 2 (red) with the L-shell concerning Enceladus' orbit and respective trajectories overlaid on ρ-Z space. (b) Positions of both Cassini (crosses) and Enceladus (filled circles) during both events on the X-Y equatorial plane. Coordinate system is the Saturn solar equatorial with X defined in the planet-Sun plane and positive toward the Sun, Z defined as the northward spin axis of Saturn, $Y = Z \times X$, and $\rho = \sqrt{(X^2 + Y^2)}$.

larger rotational speed than its conjugate footpoint at Enceladus. The longitude values are considered west longitudes derived from Davies et al. (1996) using Voyager data. Since the longitudinal separation, rather than absolute longitude, is the important value here, the choice of longitude systems is not relevant.

3. Discussion

The emission in Figure 2 can be visualized as the result of whistler mode waves with a range of frequencies launching from the same source. Each frequency propagates along a conical shell of half-angle ψ_{res}, which is rotationally symmetric about the source magnetic field line. The hollow V shape is an indicator that they originate from a common source. We refer the reader to Figure 3a from Gurnett et al. (2011) for a visual illustration of this. The V shape in Figure 2 is understandably not symmetric due to propagation effects in three dimensions. In other words, Cassini's trajectory is at some oblique angle to the source magnetic field line, as shown in Figure 1.

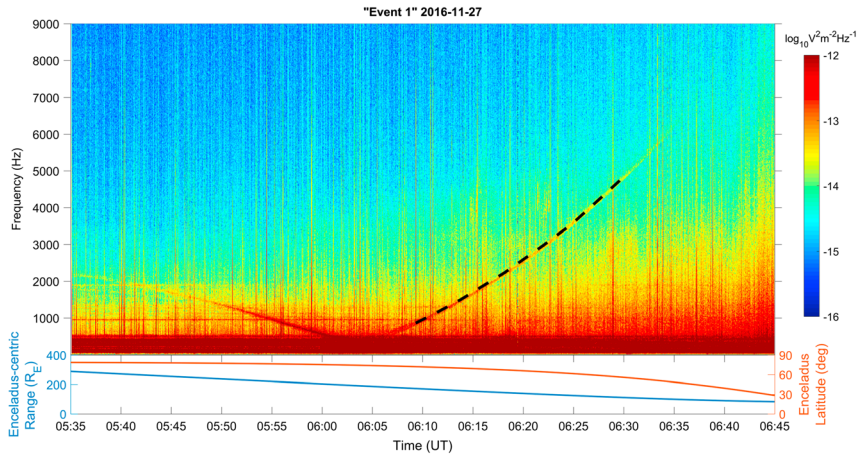

Figure 2. High-resolution electric field dynamic spectrogram of Event 1 from the wideband receiver (WBR) taken on 27 November 2016. The black dashed line corresponds to the range of frequencies used for ray-tracing analysis in Figure 3.

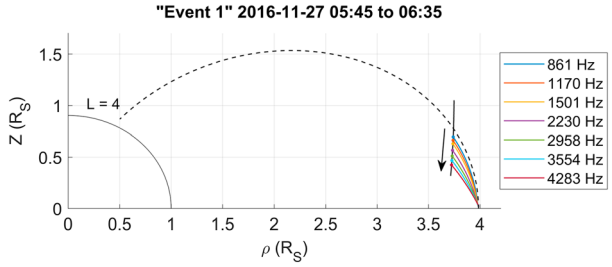

Figure 3. Ray-tracing analysis performed on Event 1 using the range of frequencies highlighted in Figure 2. Overlaid is the Enceladus flux tube at L = 4 (black dashed line) along with Cassini's trajectory (black solid line) and direction of travel (black arrow).

Simple ray-tracing analysis can compute the source of the auroral hiss by prescribing the dispersion relation in equation (1) to the range of frequencies highlighted (black dashed line) in Figure 2. Near Enceladus, f_{pe} is typically 60 kHz (Gurnett et al., 2011) and f_{ce} is typically 9 kHz (Dougherty et al., 2006). Fortunately, this means that this exercise can be greatly simplified since the region near Enceladus is that of high density ($f_{pe}^2 \gg f_{ce}^2$), which reduces equation (1) to $\sin \psi_{res} \simeq f/f_{ce}$. Therefore, recognizing that f_{ce} (Hz) = 28$|\boldsymbol{B}|$(nT), only a magnetic field model is required (Dougherty et al., 2004). The results of the ray-tracing analysis are shown in Figure 3 and projected onto ρ-Z space (coordinate system defined in the caption). Indeed, this shows that the auroral hiss is originating from Enceladus' orbit and since Figure 1b shows the event occurred when both Cassini and Enceladus were located in nearly identical longitudes, we conclude that the auroral hiss is generated from Enceladus-sourced plasma instabilities.

The spectrogram in Figure 4 (Event 2), on the other hand, shows a more complex structure of the auroral hiss compared to that of Event 1. Here Cassini was also on the same L-shell connected to Enceladus and at a time when they were in both similar longitudes. However, this feature was captured for the first time at a remote location from Enceladus, particularly at high latitude and very close to Saturn. The magnetic field exhibits a strong azimuthal, B_ϕ, component indicative of field-aligned currents at 12:21. We determine the ionospheric meridional current required to close the B_ϕ signature through Ampère's law (e.g., Hunt et al. (2014)). The gradients in the meridional current are interpreted as a downward followed by an upward directed field-aligned current with respect to Saturn's northern ionosphere. The associated current densities are ~225 and ~200 nA m^{-2} for the downward and upward segments, respectively. The slight difference is due to the negative gradient in the meridional (upward) current occurring over a slightly larger range of latitudes and therefore a wider magnetic field region. The width of the flux tube is much narrower than that of the emission, and this is due to the waves propagating obliquely to the source flux tube, thus covering a larger angular range. Note that the magnetic field instrument undergoes a range change at 12:21:52, just after the sharp peak, hence generating some digitization noise.

The region close to the planet is highly magnetized such that $f_{ce}^2 \gg f_{pe}^2$. This condition also holds during Event 2 when Cassini was approximately an hour from closest approach. Throughout the close passes of Saturn, the electron density was measured up to 1,000 cm^{-3} (Wahlund et al., 2018) and the peak magnetic

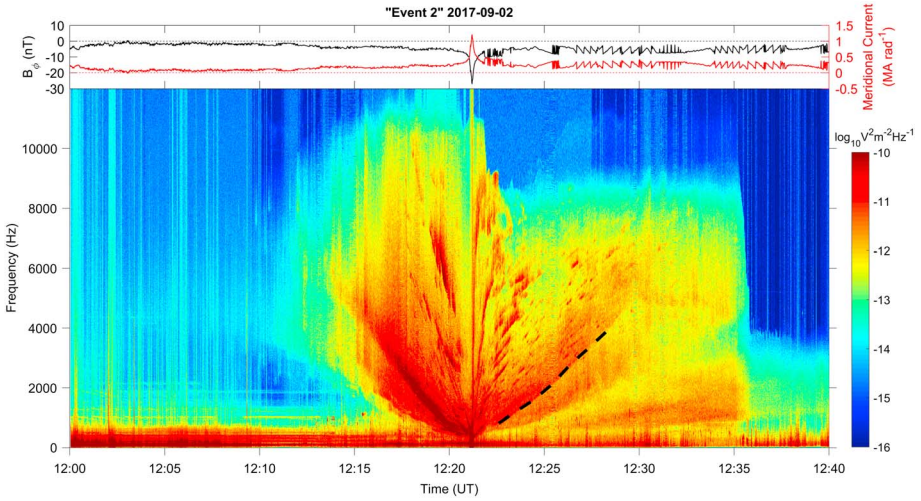

Figure 4. High-resolution electric field dynamic spectrogram of Event 2 from the wideband receiver taken on 2 September 2017. The black dashed line corresponds to the range of frequencies used for ray-tracing analysis in Figure 4. Panel above is the B_ϕ component of the magnetic field (black) and inferred meridional current per radian of azimuth (red).

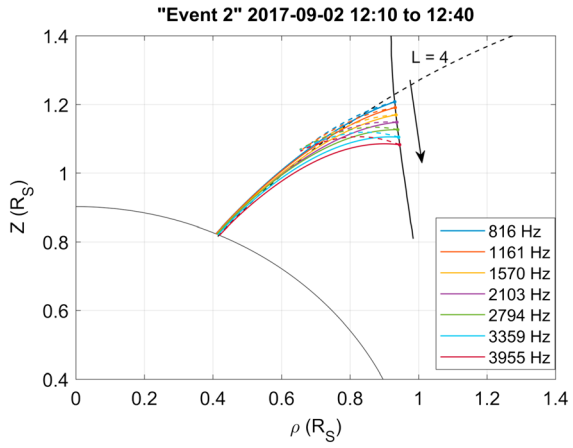

Figure 5. Ray-tracing analysis performed on Event 2 using the range of frequencies highlighted in Figure 4. The solid lines are paths of the corresponding frequencies employing one standard deviation above the average density profile, whereas the dashed lines are those employing the average density profile. Overlaid is the Enceladus flux tube at L = 4 (black dashed line) along with Cassini's trajectory (black solid line) and direction of travel (black arrow).

field strength was over 18,000 nT. The upper frequency cutoff on Figure 4 is therefore believed to be f_{pe}. There are several notable features in the form of sharp dropouts in the upper cutoff. First, at 12:21, there appears to be sharp dropouts on either side of the Enceladus flux tube. This is consistent with Cassini's traversal of the flux tube edges as indicated by the magnetic field data. Second, the dropout at 12:22 is probably due to a local density cavity. What remains unclear is whether the density is constant until 12:36 or variable as shown by the faint broadband emission around 12:25 indicating an enhancement above 8 kHz. Finally, the largest dropout of over a factor of 3 occurs at 12:36 and these are a consistent feature seen during the Grand Finale orbits on L-shells connected to the A and B rings. Farrell et al. (2018, this issue) associated these depletions with evacuated A- and B-ring-connected flux tubes setting up ambipolar effects which, in turn, retard electron outflow. It is worth noting that Cassini crosses a large range of L-shells in a short period of time due to its both high speed and high inclination. In this time history, the L-shells ranged from 7.6 to 2.1.

Figure S1 is a spectrogram of Event 2 from the five-channel WFR showing high power in the electric field and no detectable power in the magnetic field. We conclude that the emissions are therefore quasi-electrostatic and thus propagating along the resonance cone. Ray-tracing analysis is performed here to determine the location of the source with respect to the spacecraft. Since $f_{ce}^2 \gg f_{pe}^2$, this reduces equation (1) to $\sin \psi_{res} \simeq f/f_{pe}$, and recognizing that f_{pe} [Hz] = 8,980 $\sqrt{n_e}$ [cm^{-3}], an ionospheric density model is required for our analysis. This has been obtained from Persoon et al. (2018, this issue), where they derived an empirical model of the density variation with altitude. There is a stark asymmetry between the northern and southern ionospheric density models owing to ring shadowing effects, and for the purpose of this work, we employ the model that describes the northern hemisphere. This is a simple two-part exponential fit to averaged data, and the mean (μ) is given by $n_e = 80915e^{(-h/545)} + 195e^{(-h/4780)}$, where n_e is the electron number density in cm^{-3} and h is the altitude in km.

Figure 5 shows the results of ray-tracing analysis performed on the range of frequencies highlighted in Figure 4 (black dashed line). The solid lines represent the paths of the frequency using one standard deviation above the mean ($\mu + \sigma$) density profile in the northern hemisphere. Inspection of the plasma frequency (the upper frequency cutoff) of Figure 4 shows that for this orbit, the densities are higher than average, and thus, the $\mu + \sigma$ density profile is better representative of this particular orbit than the mean (μ) density profile. Note that the orbit-to-orbit variability in electron density during the Grand Finale orbits is up to 2 orders of magnitude (Persoon et al., 2018, this issue; Wahlund et al., 2018). That said, we have overlaid the paths using the mean density profile as the dashed lines to demonstrate how sensitive the ray tracing is to parameters of the density model. The errors associated with the source position in this regime are nonnegligible since the raypath angles are principally dependent on the electron density. In contrast, the errors associated with the source in Figure 3 are negligible since the raypath angles are principally dependent on the magnetic field, which is represented more accurately by its model and has much lower variability compared to the electron density near the ionosphere.

There are two possibilities for the source region of this event: at Saturn's ionosphere or at Enceladus. In addition to the ray-tracing results showing convergence toward Saturn, visual inspection also supports this conclusion by indicating that the fine structures appear preserved and the power in the electric field is high. The emission also appears fully developed. If this were coming from Enceladus, we would expect the structures to be more diffuse and the electric field power to be much fainter, if not completely damped. Moreover, the upper frequency cutoff would be expected to be much lower, thus "trimming" most of the structure as it is unlikely that the density is constantly high enough between Enceladus and Saturn to allow the waves to propagate all the way to Saturn unhindered. Indeed, ray tracing shows no convergence when the waves are assumed to originate from Enceladus.

The most apparent detail of this spectral feature is that it is not the familiar V-shaped emission as seen in Event 1 and other works concerning auroral hiss at Enceladus (e.g., Leisner et al., 2013). The explanation

here is that the feature can be thought of as originating from a series of sources along the field line. Each source launches a range of frequencies that propagate along conical shells of their corresponding range of half-angles, creating a single V shape in the spectrogram. The variable distance between the spacecraft and each source leads to the nested V shapes in the spectrogram. The narrower the V shape, the closer the spacecraft was to the source, and vice versa. The source is therefore more like an extended continuum launching whistler mode emissions that are guided along the Enceladus flux tube. These propagate from Saturn's ionosphere in the same sense as upgoing electrons, that is, downward currents, responsible for completing the current loop between Enceladus and Saturn. This field-aligned current system, known as Alfvén current tubes, was put forth by Drell et al. (1965) and extended by Neubauer (1980) to explain the electrodynamic interaction between Jupiter's magnetosphere and Io. Indeed, during a close flyby of Io, the plasma wave instrument onboard the Galileo spacecraft detected an auroral hiss signature similar to those detected near Enceladus (Xin, Gurnett, & Kivelson, 2006) and are believed to be of the same nature.

Pryor et al. (2011) reported two observations of the Enceladus auroral footprint in the northern hemisphere using Cassini's Ultraviolet Imagine Spectrograph (UVIS) instrument. They found the locations of both to be at a latitude of ~64° and each having a longitudinal separation with Enceladus of 1.7° and 0.8°, respectively. Event 2 is in excellent agreement with the location of the previously observed auroral footprint. The whistler waves converge near the 1-bar level at a latitude of 63° on Saturn's ionosphere. In addition, Figure 1b shows that Enceladus similarly had a small longitudinal separation from the event. For this particular event, no concurrent Enceladus auroral footprint signature was observed by the UVIS instrument (W. R. Pryor, personal communication, May 18, 2018). While both the auroral footprint and auroral hiss are associated with the same flux tube connected to Enceladus, the auroral footprint is generated by higher-energy particles than those that generate the auroral hiss. For this reason, they do not necessarily have to occur concurrently.

4. Summary and Conclusion

We have presented two events of auroral hiss emissions during Cassini's traversal of flux tubes connecting Saturn to Enceladus. Both events occurred when Enceladus was in the same longitude as Cassini. Event 1 was recorded during a near-equatorial close encounter with the icy moon and exhibited the familiar V-shaped emission in the electric field frequency-time spectrogram. Ray-tracing analysis shows the emission propagating locally from a source at Enceladus. Event 2 was, for the first time, observed at a large distance from Enceladus and at both high latitude and close proximity to Saturn. The detection of the Enceladus auroral hiss close to Saturn was not only exclusively afforded by the Grand Finale orbits but also rather fortuitous as it required Cassini to traverse Enceladus' flux tube when both the spacecraft and icy satellite were in similar longitudes. The spectral feature was vastly different, manifesting as nested V shapes in the spectrogram which is indicative of an extended source region along the field line. Ray-tracing analysis revealed convergence toward Saturn at a latitude of 63°, in excellent agreement with earlier UVIS observations of the Enceladus auroral footprint (Pryor et al., 2011). This result sheds new light on the spatial extent of the electrodynamic coupling between Saturn and its icy moon as well as wave-particle processes operating between the two bodies.

Acknowledgments
Useful discussions with D. G. Mitchell, W. R. Pryor, and L. Lamy are gratefully acknowledged. We also thank the reviewers for their constructive feedback. Cassini RPWS data will be publicly available via NASA's Planetary Data System on a Project-agreed schedule. Prior to this, the data may be requested from the lead author. Data relating to the ray-tracing analyses may also be requested from the lead author. The research at the University of Iowa was supported by NASA through contract 1415150 with the Jet Propulsion Laboratory. G. J. H. acknowledges support from STFC grant ST/N000692/1.

References

Davies, M. E., Abalakin, V. K., Bursa, M., Lieske, J. H., Morando, B., Morrison, D., et al. (1996). Report of the IAU.COSPAR working group on cartographic coordinates and rotational elements of the planets and satellites. *Celestial Mechanics and Dynamical Astronomy*, *63*(2), 127–148. https://doi.org/10.1007/BF00693410

Dougherty, M. K., Kellock, S., Southwood, D. J., Balogh, A., Smith, E. J., Tsurutani, B. T., et al. (2004). The Cassini magnetic field investigation. *Space Science Reviews*, *114*(1-4), 331–383. https://doi.org/10.1007/s11214-004-1432-2

Dougherty, M. K., Khurana, K. K., Neubauer, F. M., Russell, C. T., Saur, J., Leisner, J. S., & Burton, M. E. (2006). Identification of a dynamic atmosphere at Enceladus with the Cassini Magnetometer. *Science*, *311*(5766), 1406–1409. https://doi.org/10.1126/science.1120985

Drell, S. D., Foley, H. M., & Ruderman, M. A. (1965). Drag and propulsion of large satellites in the ionosphere: An Alfvén propulsion engine in space. *Journal of Geophysical Research*, *70*(13), 3131–3145. https://doi.org/10.1029/JZ070i013p03131

Farrell, W. M., Hadid, L. Z., Morooka, M. W., Kurth, W. S., Wahlund, J.-E., MacDowall, R. J., et al. (2018). Saturn's plasma density depletions along magnetic field lines connected to the main rings. *Geophysical Research Letters*, *45*. https://doi.org/10.1029/2018GL078137

Gurnett, D. A. (1966). A satellite study of VLF hiss. *Journal of Geophysical Research*, *71*(23), 5599–5615. https://doi.org/10.1029/JZ071i023p05599

Gurnett, D. A., Averkamp, T. F., Schippers, P., Persoon, A. M., Hospodarsky, G. B., Leisner, J. S., et al. (2011). Auroral hiss, electron beams and standing Alfvén wave currents near Saturn's moon Enceladus. *Geophysical Research Letters*, *38*, L06105. https://doi.org/10.1029/2011GL046854

Gurnett, D. A., Kurth, W. S., Kirchner, D. L., Hospodarsky, G. B., Averkamp, T. F., Zarka, P., et al. (2004). The Cassini radio and plasma wave investigation. *Space Science Reviews*, *114*(1-4), 395–463. https://doi.org/10.1007/s11214-004-1434-0

Gurnett, D. A., Shawhan, S. D., & Shaw, R. R. (1983). Auroral hiss, Z mode radiation, and auroral kilometric radiation in the polar magnetosphere: DE 1 observations. *Journal of Geophysical Research*, *88*(A1), 329. https://doi.org/10.1029/JA088iA01p00329

Hunt, G. J., Cowley, S. W. H., Provan, G., Bunce, E. J., Alexeev, I. I., Belenkaya, E. S., et al. (2014). Field-aligned currents in Saturn's nightside magnetosphere: Subcorotation and planetary period oscillation components. *Journal of Geophysical Research: Space Physics*, *119*, 9847–9899. https://doi.org/10.1002/2014JA020506

James, H. G. (1976). VLF saucers. *Journal of Geophysical Research*, *81*(4), 501–514. https://doi.org/10.1029/JA081i004p00501

Kopf, A. J., Gurnett, D. A., Menietti, J. D., Schippers, P., Arridge, C. S., Hospodarsky, G. B., et al. (2010). Electron beams as the source of whistler-mode auroral hiss at Saturn. *Geophysical Research Letters*, *37*, L09102. https://doi.org/10.1029/2010GL042980

Leisner, J. S., Hospodarsky, G. B., & Gurnett, D. A. (2013). Enceladus auroral hiss observations: Implications for electron beam locations. *Journal of Geophysical Research: Space Physics*, *118*, 160–166. https://doi.org/10.1029/2012JA018213

Menietti, J. D., Averkamp, T. F., Ye, S. Y., Sulaiman, A. H., Morooka, M. W., Persoon, A. M., et al. (2018). Analysis of intense Z-mode emission observed during the Cassini proximal orbits. *Geophysical Research Letters*, *45*. https://doi.org/10.1002/2018GL077354

Neubauer, F. M. (1980). Nonlinear standing Alfvén wave current system at Io: Theory. *Journal of Geophysical Research*, *85*(A3), 1171–1178. https://doi.org/10.1029/JA085iA03p01171

Persoon, A. M., Kurth, W. S., Gurnett, D. A., Groene, J. B., Sulaiman, A. H., Wahlund, J.-E., et al. (2018). Electron density distributions in Saturn's ionosphere. *Geophysical Research Letters*, *45*. https://doi.org/10.1029/2018GL078020

Pryor, W. R., Rymer, A. M., Mitchell, D. G., Hill, T. W., Young, D. T., Saur, J., et al. (2011). The auroral footprint of Enceladus on Saturn. *Nature*, *472*(7343), 331–333. https://doi.org/10.1038/nature09928

Spahn, F., Schmidt, J., Albers, N., Hörning, M., Makuch, M., Seiss, M., et al. (2006). Cassini dust measurements at Enceladus and implications for the origin of the E ring. *Science*, *311*(5766), 1416–1418. https://doi.org/10.1126/science.1121375

Stix, T. H. (1992). *Waves in plasmas*. New York: American Institute of Physics.

Sulaiman, A. H., Kurth, W. S., Hospodarsky, G. B., Averkamp, T. F., Persoon, A. M., Menietti, J. D., et al. (2018). Auroral hiss emissions during Cassini's Grand Finale: Diverse electrodynamic interactions between Saturn and its rings. *Geophysical Research Letters*, *45*. https://doi.org/10.1029/2018GL077875

Sulaiman, A. H., Kurth, W. S., Persoon, A. M., Menietti, J. D., Farrell, W. M., Ye, S. Y., et al. (2017). Intense harmonic emissions observed in Saturn's ionosphere. *Geophysical Research Letters*, *44*, 12,049–12,056. https://doi.org/10.1002/2017GL076184

Wahlund, J. -E., Morooka, M. W., Hadid, L. Z., Persoon, A. M., Farrell, W. M., Gurnett, D. A., et al. (2018). In situ measurements of Saturn's ionosphere show that it is dynamic and interacts with the rings. *Science*, *359*, 66–68. https://doi.org/10.1126/science.aao4134

Xin, L., Gurnett, D. A., & Kivelson, M. G. (2006). Whistler mode auroral hiss emissions observed near Jupiter's moon Io. *Journal of Geophysical Research: Space Physics*, *111*, A04212. https://doi.org/10.1029/2005JA011411

Xin, L., Gurnett, D. A., Santolík, O., Kurth, W. S., & Hospodarsky, G. B. (2006). Whistler-mode auroral hiss emissions observed near Saturn's B ring. *Journal of Geophysical Research*, *111*, A06214. https://doi.org/10.1029/2005JA011432